Engineering Structures 283 (2023) 115793

Contents lists available at ScienceDirect

Engineering Structures

journal homepage: www.elsevier.com/locate/engstruct

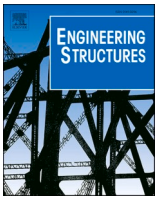

# Experimental investigation and mechanical modelling of shear failure in reinforced concrete members with plain and ribbed bent-up bars

Tobias Huber *, Franz Untermarzoner, Johann Kollegger

*Institute for Structural Engineering, Vienna University of Technology, Karlsplatz 13/212-2, 1040 Vienna, Austria*

ARTICLE INFO

*Keywords:*
Shear strength
Bent-up bars
Assessment
Existing structures
Plain reinforcing bars
Digital image correlation
Localised shear crack
Shear transfer mechanisms

ABSTRACT

Using bent-up bars as shear reinforcement was state of the art in reinforced concrete (RC) construction until the 1970s. Since the approach to shear reinforcement design has changed since then, the structural assessment according of structural members to current structural codes often yield insufficient theoretical shear capacities. In this paper, a series of twelve shear tests on members with plain and ribbed bent-up bars is presented. Despite the beams only containing plain bars or widely spaced bent-up bars, the test results show higher shear capacity compared to reference beams without any shear reinforcement, and the formation of pronounced localised shear cracks. The contribution of the bent-up bars to the shear strength is evaluated by combining the constitutive laws of various shear transfer mechanisms along an idealised shear crack. The model approach is validated by a comparison with detailed test measurements. It is shown that the interaction of the bent-up reinforcing bars with other shear mechanisms in a localised shear crack is highly dependent on the bond behaviour of bent-up and longitudinal bars. The great potential of this approach for the refined assessment of existing structures with bent-up bars is confirmed by the accuracy of its predictions.

## 1. Introduction

Bent-up bars have been used widely since François Hennebique introduced them in 1893. Longitudinal reinforcing bars can be bent up in areas where they are no longer needed to transfer tension forces resulting from the bending moment. The inclined part of the reinforcement then serves as shear reinforcement (Fig. 1a). Nowadays, bent-up bars are commonly found in deck slabs of box girders (Fig. 1b) or in punching reinforcement (Fig. 1c). According to Mörsch's [1] first design recommendations based on early test series of beams with plain bent-up bars [2,3], the bars were usually bent at an angle of 45° to resist the principal tensile stresses in the area of the supports. Similar rules about the design of bent-up bars, based on [4], were developed in the United States. This procedure was considered state of the art for a long time, up until Leonhardt [5] showed, by way of tests on RC beams, that stirrups offer more advantages than bent-up bars in terms of shear crack widths. In addition, the danger of longitudinal splitting in the areas where the inclination of the reinforcing bars changes was considered significant, which is why it was recommended to encircle the bars with stirrups. Despite their structural efficiency, bent-up bars have become less common since the 1960s, because of the effort needed for the bending and placing of such bars. For this reason, the shear resistance and structural behaviour of members with bent-up bars have received limited attention by the research community. Only a few test series from the 1970s of members with bent-up bars with bending angles between 30° and 60° are available [6–8]. Other studies focussed on the load-bearing behaviour [9,10] and the application of the theory of plasticity to beams with bent-up bars [11].

Current design codes are commonly based on truss models with fixed [12] or variable [13] concrete strut inclination or on the compression field theory [14,15]. The truss models assume the formation of equally inclined concrete struts which are held together by smeared tension struts. This means that the tension struts (the shear reinforcement) need to be spaced reasonably closely to prevent localised shear cracking. As a result, the spacing limits for bent-up bars are often problematic in existing structures, which were usually designed with wider spacings. This issue was recently addressed using a semi-empiric model [16,17] based on experimental investigations of the shear behaviour of members containing ribbed bent-up bars in various reinforcement layouts [18]. The model evaluates the contributions to the shear strength of concrete and steel inside a localised crack, similar to the concept followed by ACI318 [12] and CEP-FIP Model Code 78 [19]. The model has been included in the Austrian code for bridge assessment [20]. The other

* Corresponding author.
*E-mail address:* tobias.alexander.huber@tuwien.ac.at (T. Huber).

https://doi.org/10.1016/j.engstruct.2023.115793
Received 9 October 2022; Received in revised form 8 January 2023; Accepted 8 February 2023
Available online 27 February 2023

**Nomenclature**

| | |
|---|---|
| $A_s$ | Cross-section area of the reinforcement |
| $E$ | Young's modulus |
| $D_{max}$ | Maximum aggregate size |
| $F$ | Force; point load |
| $M$ | Bending moment |
| $V$ | Shear force |
| $V_{Agg}$ | Contribution of aggregate interlock to the shear strength |
| $V_{Compr}$ | Contribution of compression chord to the shear strength |
| $V_{Res}$ | Contribution of residual tensile stresses in the fracture process zone to the shear strength |
| $V_{Dow}$ | Contribution of dowel action of the longitudinal reinforcement to the shear strength |
| $V_{Exp}$ | Maximum shear strength in the experiment |
| $V_{SD}$ | Contribution of dowel action of the bent-up bar to the shear strength |
| $V_{ST}$ | Contribution of tensile force action of the bent-up bar to the shear strength |
| $V_{Stir}$ | Contribution of the stirrups to the shear strength |
| $V_{Mod}$ | Shear resistance according to the model |
| $a$ | Shear span (distance between support and point load) |
| $b$ | Width |
| $c$ | Compression zone depth; cement |
| $d$ | Static depth of the beam |
| $d_s$ | Bar diameter |
| $f_c$ | Concrete cylinder compressive strength |
| $f_{ct}$ | Tensile strength of the concrete |
| $f_t$ | Tensile strength of the reinforcing bar |
| $f_y$ | Yield strength of the reinforcing bar |
| $h$ | Height of the structural member |
| $l$ | Length |
| $l_B$ | Length contributing to shear crack opening |
| $m$ | Mean value |
| $s$ | Sliding within a crack plane |
| $s_b$ | Crack width perpendicular to the axis of the bent-up bar |
| $s_{bu}$ | Spacing of bent-up bars parallel to the longitudinal reinforcement |
| $w$ | Crack width perpendicular to the crack plane |
| $w_b$ | Crack width parallel to axis of the bent-up bar |
| $u$ | Horizontal opening; i.e. the horizontal distance between opposite crack faces |
| $v$ | Vertical opening; i.e. the vertical distance between opposite crack faces |
| $x_A$ | Distance of the crack origin from the support |
| $z$ | Inner lever arm |
| $\Sigma V_i$ | Sum of the contributions of the various shear transfer actions |
| $\alpha$ | Angle of the inclined portion of the bent-up bar |
| $\beta$ | Idealised crack angle |
| $\delta$ | Relative displacement |
| $\delta_b$ | Bond slip |
| $\varepsilon_s$ | Reinforcement strain |
| $\rho_w$ | Shear reinforcement ratio |
| $\rho_{w,\min}$ | Minimum shear reinforcement ratio according to structural codes |
| $\tau_b$ | Bond stress |

*Abbreviations*

| | |
|---|---|
| ACDM | Automatic crack detection and measurement |
| COV | Coefficient of variation |
| DIC | Digital image correlation |
| LVDT | Linear variable differential transformer |
| RC | Reinforced concrete |
| PL | Plain |
| RI | Ribbed |
| SG | Strain gauge |

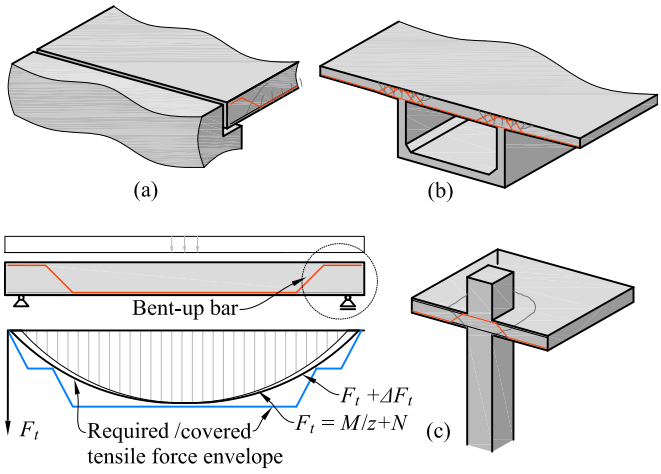


**Fig. 1.** Typical applications of bent-up bars: (a) slab bridge and design principle of bent-up bars in RC members; (b) deck slab of a box girder bridge; (c) punching of a floor slab.

major problem in the assessment of the shear capacity is that current codes and their models are generally only applicable to structures built with ribbed reinforcing bars. Although plain reinforcing bars are hardly used any more, it is important to understand their behaviour, as many structures built with plain reinforcing bars are still in use (in East Germany, for example, plain reinforcing bars were commonly used until 1990). The present paper aims to shed light on the shear behaviour of bent-up bars by investigating the effect of using plain instead of ribbed reinforcing bars in RC structures.

## 2. Experimental investigation

### 2.1. Specimens and test set-up

In this section, the main results of a test series on seven reinforced concrete beams are presented. The details of the beams (dimensions and reinforcement layout) are summarised in Fig. 2 and Table 1. The specimens were labelled with an identifying code: the first letter corresponds to the bar type of the bent-up bars (PL = plain, RI = ribbed), the following number refers to the bar diameter $d_s$ in millimetres, and the subsequent number indicates the shear reinforcement ratio of the stirrups in thousandths, calculated with $\rho_w = A_s/(b{\cdot}s{\cdot}\sin\alpha)$. The additional letters indicate either the use of ribbed longitudinal reinforcing bars (R) or that the bent-up bars were spaced more closely than in the reference configuration (n).

The depth $h$ and width $b$ of the members were 550 mm and 500 mm, respectively. The longitudinal reinforcement consisted of three bars Ø30 running along the entire length of the specimen and two or three additional bars, some of which were bent up. As a result, the longitudinal reinforcement ratio $\rho$ changes along the length of the member ($\rho$ = 0.85–1.49 %). Short transverse bars Ø12/200 mm were placed underneath the main longitudinal reinforcement. Considering the concrete cover (25 mm), the static depth $d$ is approximately 500 mm. Three

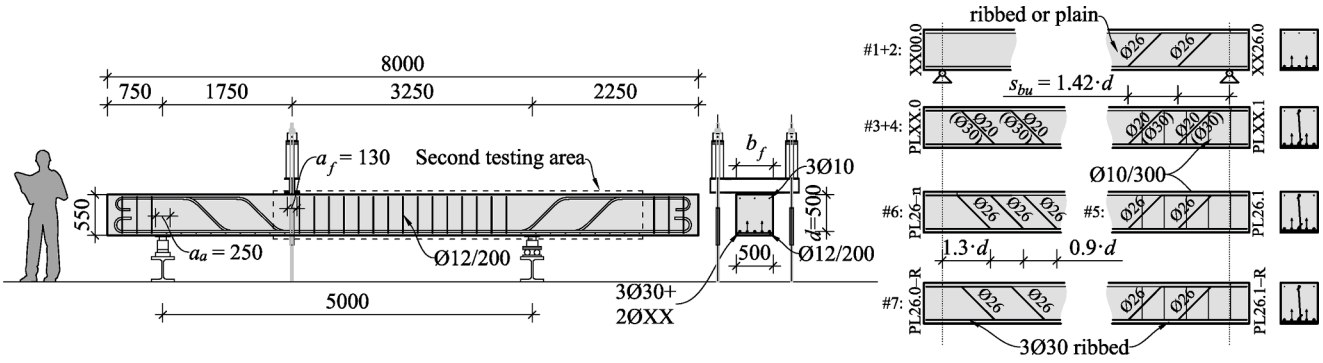


**Fig. 2.** Test set-up and specimen details for shear tests with bent-up bars.

**Table 1**
Details of reinforcement, mechanical properties of concrete and experimentally determined shear strength.

| Specimen | | Longitudinal reinforcement | Bent-up bars | Stirrups | $\rho_w$ (%) | $f_c$ (MPa) | $f_{ct}$ (MPa) | $E_c$ (GPa) | $V_{Exp}$ (kN) | $V_{Exp}/V_{Exp,PL00.0}$ |
|---|---|---|---|---|---|---|---|---|---|---|
| 1 | PL00.0 | 3Ø30 + 2Ø26 (plain) | — | — | — | 38.6 | 3.33 | 33.0 | 252.6 | — |
| | PL26.0 | 3Ø30 (plain) | 2Ø26@710 (plain) | — | 0.212 | | | | 342.5 | 1.36 |
| 2 | RI00.0 | 3Ø30 + 2Ø26 (ribbed) | — | — | — | | | | 253.4 | 1.00 |
| | RI26.0 | 3Ø30 (ribbed) | 2Ø26@710 (ribbed) | — | 0.212 | | | | 445.5 | 1.76 |
| 3 | PL20.0 | 3Ø30 (plain) | 2Ø20@710 (plain) | — | 0.125 | 41.7 | 3.64 | 34.1 | 260.7 | 1.03 |
| | PL20.1 | 3Ø30 (plain) | 2Ø20@710 (plain) | 1Ø10@300 | 0.178 | | | | 291.2[a] | 1.15 |
| 4 | PL30.0 | 3Ø30 (plain) | 2Ø30@710 (plain) | — | 0.282 | | | | 351.9 | 1.39 |
| | PL30.1 | 3Ø30 (plain) | 2Ø30@710 (plain) | 1Ø10@300 | 0.334 | | | | 392.9[a] | 1.56 |
| 5 | PL26.1 | 3Ø30 (plain) | 2Ø26@710 (plain) | 1Ø10@300 | 0.264 | 40.9 | 3.38 | 33.7 | 347.6[a] | 1.38 |
| 6 | PL26.0–n | 3Ø30 (plain) | 3Ø26@450[b] (plain) | — | 0.334 | | | | 380.2[a] | 1.51 |
| 7 | PL26.0–R | 3Ø30 (ribbed) | 2Ø26@710 (plain) | — | 0.212 | 39.8 | 3.47 | 32.6 | 283.6 | 1.12 |
| | PL26.1–R | 3Ø30 (ribbed) | 2Ø26@710 (plain) | 1Ø10@300 | 0.264 | | | | 360.0 | 1.43 |

[a] Flexural failure.
[b] First bent-up bar at 650 mm from support

longitudinal ribbed bars Ø10 were placed in the compression zone of the beams. The reinforcement layout varied at each end of the beams, typically consisting of two bent-up bars at a spacing of 1.42·$d$ or three bent-up bars at a spacing of 0.9·$d$. In some beams, one-legged plain stirrups Ø10 were added at the ends. The total amount of shear reinforcement was chosen to result in a reinforcement ratio of 0.8–2.3 times the minimum reinforcement ratio $\rho_{w,\min} = 0.08\sqrt{f_c}/f_{yw}$ specified in [15]. For the material properties of the beams of this test series, this formula results in a shear reinforcement ratio of 0.17 ‰. In two reference beams, the ends did not contain any shear reinforcement. The shear reinforcement outside the testing areas consisted of two-legged ribbed stirrups Ø12/200 mm. The ends of all plain reinforcing bars were bent to form hooks in order to ensure appropriate anchorage.

The test set-up is shown in Fig. 2. The members were loaded with a point load applied at $a = 3.5{\cdot}d$ from one end of a simply supported span of length 10·$d$. To prevent any damage to the second testing area, this part of the beam was cantilevering out over the support during the first test. The loading plates under the hydraulic jack and the support plates had the same width $b_f$ as the specimens (500 mm) but differed in length ($a_a = 250$ mm and $a_f = 130$ mm, respectively). The support plates were placed on spherical caps, which at one support were supplemented by rollers, thus permitting rotation as well as longitudinal displacements.

### 2.2. Material properties

#### 2.2.1. Reinforcement

To obtain different bond behaviours, both conventional ribbed reinforcing bars (class B550B) and plain reinforcing bars were used. Various classes of plain bars were used both for the shear reinforcement (bent-up bars and stirrups) and the longitudinal reinforcement (3Ø30). For the shear reinforcement, class S235JR + AR (#1.0038) was used, which is equivalent to class St37 of past German standards for structural concrete. To avoid premature flexural failure, alloy bars of class S460 (#1.5217) with a higher target yield point were used as the longitudinal reinforcement. Three tension tests were conducted to determine the mechanical properties of the bars of the various steel diameters (sample length 1.1 m). Table 2 shows a summary of the obtained material parameters.

#### 2.2.2. Concrete

The concrete with a maximum aggregate size of 16 mm was designed

**Table 2**
Mechanical properties of reinforcing bars.

| Type | Surface | $Ø_{eff}$ (mm) | $A_s$ (mm$^2$) | $f_y$ [a] (MPa) | $f_t$ (MPa) | $A_{gt}$ (%) | $E_s$ (GPa) | $\overline{\tau_b}$ [b] (MPa) |
|---|---|---|---|---|---|---|---|---|
| Ø10-S235 | Plain | 10.12 | 80.5 | 336 | 402 | 22.7 | 210.0 | — |
| Ø20-S235 | Plain | 20.03 | 315.3 | 328 | 464 | 24.9 | 204.5 | 1.04 |
| Ø26-S235 | Plain | 26.10 | 535.1 | 304 | 457 | 24.6 | 204.9 | 0.76 |
| Ø30-S235 | Plain | 30.07 | 710.2 | 294 | 460 | 27.6 | 201.2 | 0.84 |
| Ø26-B550B | Ribbed | — | 530.9 | 574 | 677 | 9.3 | 204.6 | — |
| Ø30-S460 | Plain | 30.05 | 709.2 | 562 | 733 | 10.1 | 208.9 | 0.38 |

[a] Offset yield point at 0.2% strain.
[b] RILEM test acc. to [21].

**Table 3**
Composition of concrete (amounts in kg/m$^3$).

| | $m$ (kg/m$^3$) |
|---|---|
| Sand 0/4 | 1013 |
| Fine gravel 4/8 | 486 |
| Coarse gravel 8/16 | 527 |
| CEMI 52.5R | 235 |
| Superplasticiser | 1.65 |
| Water | 160 |

to have a target compressive strength $f_c$ of 40 MPa. Cement class CEMI was used and the resulting water–cement ratio $w/c$ was 0.68. The detailed composition of the concrete is shown in Table 3. Two beams were cast per day, and additional samples were cast to determine the material properties of the concrete. The material properties are listed in Table 1. Compression tests on three cylinders ($h/Ø$ = 300/150 mm) were used to determine the mean compressive strength $f_c$ and the compressive modulus of elasticity $E_c$. The uniaxial tensile strength $f_{ct}$ of the concrete was obtained from a standard Brazilian test (determined on three cylinders: $h/Ø$ = 300/150 mm).

### 2.2.3. Bond tests

The bond behaviour between the plain reinforcing bars and the concrete was obtained by executing pull-out tests as specified in RILEM [21]. Three tests were conducted for each of the various diameters of bent-up or longitudinal bars. The specimen dimensions were different for each bar diameter (cube with a = 10·$d_s$; sheath length = 5·$d_s$). The obtained values of the mean bond stress $\overline{\tau_b}$ are listed in Table 2.

## 2.3. Measurements

The applied loads were measured both by load cells at the hollow-piston jacks and two load cells at each support. The strains within the bent-up bars were measured by two strain gauges applied directly to two opposite sides of the bar, at the centre of the inclined portion. The deformations on each beam surface were determined by digital image correlation (DIC). One side of the beam was observed with a stereo system containing two cameras (2352 × 1728 px resolution,

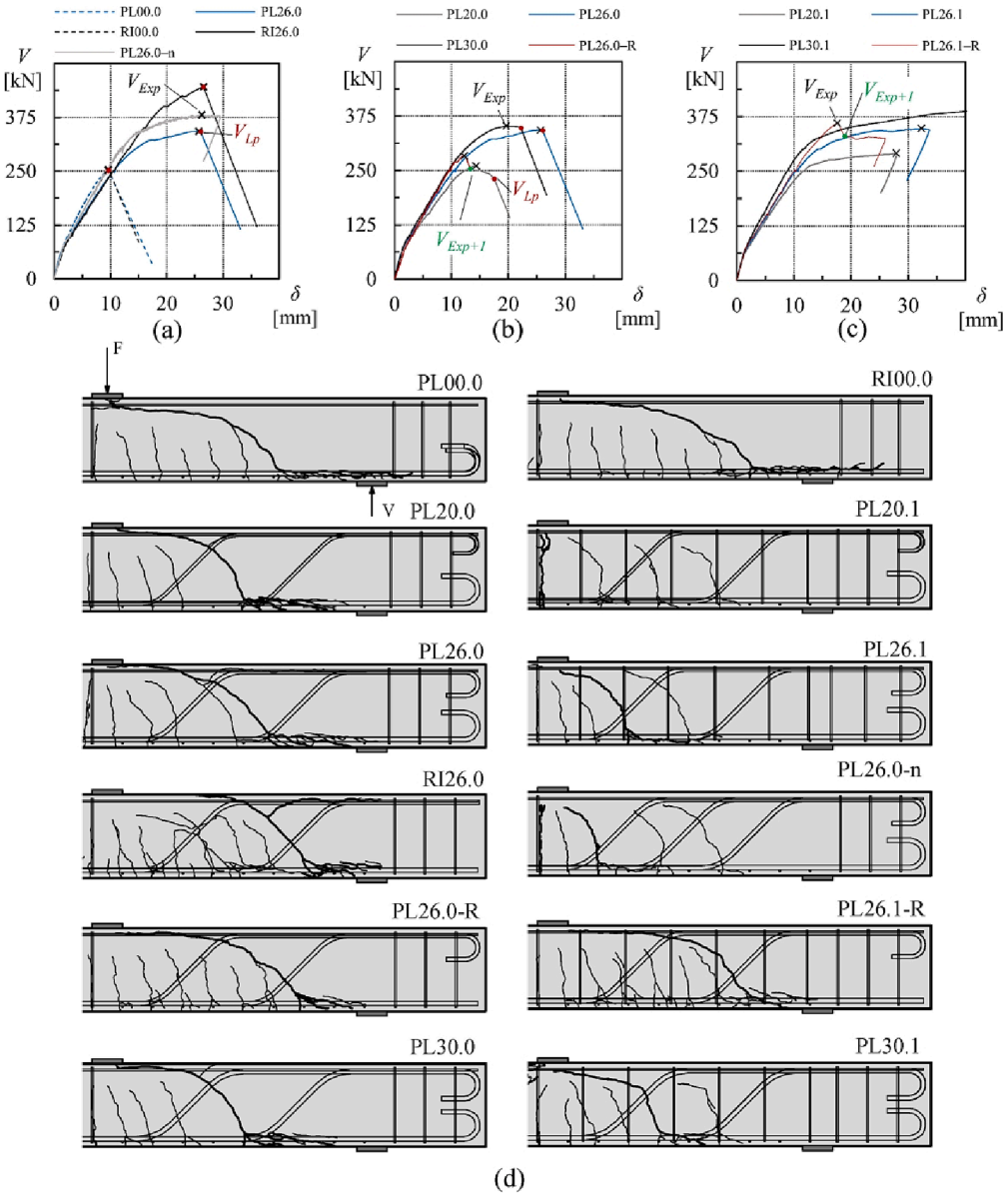


**Fig. 3.** Shear force vs relative deflection for: (a) beams with ribbed and plain reinforcement; (b) beams with plain bent-up bars; (c) beams with additional stirrups; (d) post-failure crack pattern for all specimens.

measurement rate 1 Hz at failure), while a standard SLR camera (4928 × 3264 px, 0.2 Hz) was used on the other side. The crack widths were determined from the measurements using automatic crack detection and measurement (ACDM) [22,23]. The deflections were determined by several LVDTs positioned underneath the specimens.

### 2.4. Test results

In Fig. 3, the measured shear force $V$ within the testing area is plotted against the relative deflection $\delta_{rel}$ between the load introduction point and the deformed supports. Table 1 shows a summary of the maximum shear strength $V_{Exp}$ determined from the tests and the comparison to the unreinforced reference beams ($V_{Exp}/V_{Exp,PL00.0}$). All tested specimens with bent-up bars exhibit higher shear strength than their reference beam. The use of different bar surface types (ribbed and plain) seemed to have no effect on the shear strength and load-deformation behaviour of the reference members (PL00.0 and RI00.0 in Fig. 3a). In contrast, the beam with ribbed bent-up bars (RI26.0) showed a 30 % increased shear strength compared to its counterpart with plain bars (PL26.0), very likely due to the higher yield point of the ribbed bars. The deflection at failure, however, was the same for both beams (Fig. 3a). The influence of the bar diameter (PLXX.0) is clearly seen in the higher shear strengths in the samples with greater-diameter bars (Fig. 3b). Interestingly, specimen PL20.0 showed only a slight increase in shear strength (3 %) compared to the reference beam (PL00.0). This might be because the shear reinforcement ratio in this beam ($\rho_w$ = 0.13 %) was below the minimum reinforcement ratio ($\rho_{w,\min}$ = 0.15 %) required by [15]. It should be noted that the shear strength of specimen PL30.0 is only slightly higher (by 3 %) than that of beam PL26.0 (further discussed in Section 4).

The investigated inclusion of a small number of stirrups ($\rho_{w,stirrups}$ = 0.053 %) (PLXX.1(–R)) has a positive effect, as it increases the shear capacity compared to the corresponding beams without any stirrups (PLXX.0(–R)). The specimens with ribbed longitudinal reinforcement exhibited a shear capacity that was 76 kN (27 %) higher than that of the reference beams, while in the specimens with smooth longitudinal bars the increase in shear capacity was limited (1–12 %) due to a change in failure mode (Fig. 3c). General conclusions about the influence of the spacing of the bent-up bars are omitted, since the full shear capacity of specimen PL26.0–n ($s_{bu}$ = 0.9·$d$) could not be reached due to prior yielding of the longitudinal reinforcement. Nevertheless, a higher shear force (+11 %) was sustained compared to PL26.0 ($s_{bu}$ = 1.42·$d$).

The effect of using ribbed longitudinal reinforcement with plain bent-up bars (PL26.X–R) is enormous, as shown by comparisons with the specimens with smooth longitudinal reinforcement (PL26.X in Fig. 3b, c). Specimen PL26.0–R exhibited a 17 % lower shear capacity than beam PL26.0 and showed no early signs of failure (Fig. 3b). Even beam PL26.1–R with its additional stirrups showed only a small increase in shear capacity (5 %) compared to beam PL26.0.

Three different failure modes were observed. Beams without shear reinforcement (PL00.0 and RI00.0) exhibited typical brittle diagonal tension failure. At the maximum shear force $V_{Exp}$, the governing shear crack showed a pronounced curved shape with only a small portion extending into the compression chord, followed upon failure by unstable crack propagation towards the load introduction point. In the beams with two bent-up bars (PLXX.0(–R); RIXX.0) and in PL26.1–R the crack shape was similar, but the crack was quite pronounced even before failure occurred. In these beams, brittle diagonal tension failure occurred but with a decrease in stiffness ahead of failure shown in the load–deflection curves. It should be noted that this decrease was more pronounced in specimens with smooth longitudinal reinforcement. In contrast, beams with stirrups (PLXX.1) or with an additional bent-up bar (PL26.0–n) exhibited flexural failure characterised by the yielding of the longitudinal reinforcement.

Fig. 3d shows the relevant post-failure crack patterns. The results show a clear dependency of the crack spacing on the bar type used.

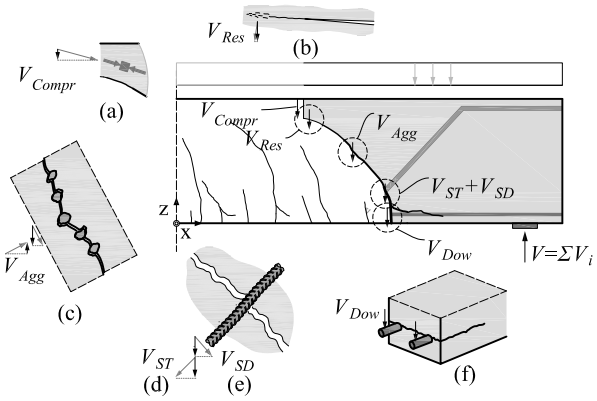


**Fig. 4.** Evaluation of shear transfer mechanisms on a free body: (a) concrete compression chord ($V_{Compr}$); (b) residual tensile stresses at the crack tip ($V_{Res}$); (c) aggregate interlock ($V_{Agg}$); (d) tensile force ($V_{ST}$) and (e) dowel action ($V_{SD}$) of the bent-up bar; (f) dowel action of the longitudinal bars ($V_{Dow}$).

Beams with ribbed longitudinal bars exhibited a denser crack pattern (RIXX.0; PL26.X–R). In contrast, the beams with plain longitudinal bars (PLXX.X), showed fewer but more pronounced cracks and wider crack spacings. Only the reference member with plain bars (PL0.00) showed small crack spacings, very likely due to the short bars placed in the transverse direction acting as crack initiators. However, the crack widths were small and remained more or less constant during the entire test procedure. No correlation between the investigated influencing parameters (bar type, bar diameter, spacing) and the location and general shape of the governing shear crack was found. This is highly important for the resulting crack kinematics and hence for the activation of the various shear transfer mechanisms, as discussed in the next section. Details of other measurement results (crack widths, bent-up bar activation) are given in the following sections.

## 3. Modelling the shear behaviour of bent-up bars inside a localised crack

### 3.1. Introduction

The shear behaviour of bent-up bars in beams exhibiting localised cracking is essentially defined by the interaction of various shear transfer mechanisms [24] (e.g. in Fig. 4a–f: concrete compression strut $V_{Compr}$, residual tensile stresses at crack tip $V_{Res}$, aggregate interlock $V_{Agg}$, tensile force $V_{ST}$ and dowel action $V_{SD}$ of the bent-up bar and dowel action of the longitudinal bars $V_{Dow}$). Since the characteristics of the individual shear transfer mechanisms essentially depend on the crack pattern, the crack shape and the associated kinematics of the crack, the formulation of a consistent model with a physical background is also very complex. In recent years, digital image correlation has allowed the shear crack kinematics as well as the strain state to be continuously recorded in high resolution [25–27]. This permits the evaluation of individual mechanisms using constitutive models of the mechanisms from the literature [18,27,28,29,30,31].

Based on these novel types of analyses, new models for prestressed concrete beams [32] and structures without shear reinforcement [33] have been developed, although different mechanisms are relevant in different structural elements. For example, aggregate interlock is essential for RC structures without shear reinforcement [26,27,29,31], while it plays a negligible role in prestressed concrete structures [32]. These evaluations further show that a redistribution between the above described mechanisms takes place for slender members without or with a low amount of shear reinforcement: aggregate interlock only becomes significant in the final stages of experiments [27,34,36] with crack propagation in the compression zone providing necessary sliding in steep crack parts for activation. The role of stress transfer and crack

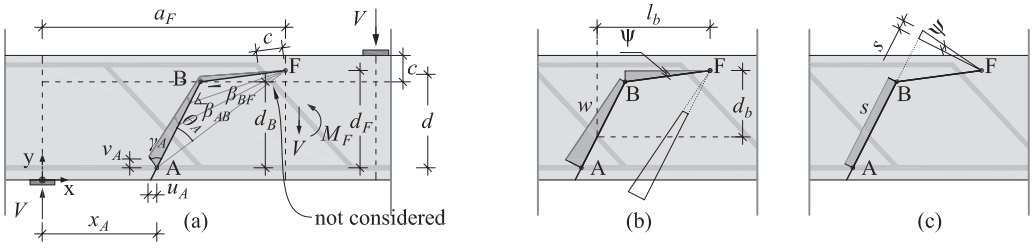


**Fig. 5.** (a) Kinematics and displacements of the crack planes according to a bilinear idealised crack; (b) crack with *w* and (c) crack sliding *s*.

propagation at the region of the uncracked compression zone for the shear failure process was recently analysed by Classen [36], also addressing the interaction of shear transfer mechanisms. While in [36] a mechanical consistent description for shear failures is given based on a bi-axial stress state in the compression zone, it is also stated that the contribution assigned to the compression zone by previous models (e.g. the semi-empirical approach of [33,34]) are not contradicted by the approach. Cavagnis [33,34] proposed a mechanical model for the shear resistance of RC concrete members without shear reinforcement based on the evaluation of constitutive laws for various shear transfer mechanisms. Similar approaches were followed by other researchers [35,36]. The shear crack geometry is idealised to consist of a quasi-vertical part and a quasi-horizontal branch. The general approach has also been illustrated in [34] for beams with a low amount of shear reinforcement, since failure can also be defined as occurring at the opening of a pronounced flexural shear crack. A similar approach was recently proposed by Tung et al. [37] for RC beams with a small amount of shear reinforcement. They also addressed the link of crack propagation with the cause of failure.

In the present study, it is shown that the shape of the governing cracks in beams with widely spaced bent-up bars (plain or ribbed) is similar to that in beams not containing any shear reinforcement. This had previously been shown in [18] for beams with ribbed bars. For this reason, the modelling approach of [33,34] is extended to structural members containing bent-up bars.

### 3.2. Shear crack shape

The following model assumptions have been taken from [34]. The model assumes a critical shear crack, the geometry of which is idealised to consist of a quasi-vertical segment (A–B) and a quasi-horizontal portion (B–F) (see Fig. 5).

The inclination of the quasi-vertical part is dependent on the moment-to-shear ratio calculated as

$$\beta_{AB} = \frac{\pi}{4} \cdot \left(1 + \frac{\alpha_A^{1/3}}{3}\right) \tag{1}$$

where $\alpha_A = M_F / (V \cdot d)$ is the shear slenderness ratio.

The end point B is defined as the location where the crack reaches the compression zone height *c* (Fig. 5a). To account for the crack characteristics of members with bent-up bars, a geometry for the portion B–F is proposed that differs from that used in [34]. In accordance with the observations made in the presented tests and in those reported in [18], the quasi-horizontal part has a fixed length $l_F = d$ and is inclined by $\beta_{BF} = \pi/20$ from point B onwards. The original model for members without shear reinforcement suggests $l_F = d/6$ and $\beta_{BF} = \pi/8$. It should be noted that the chosen geometry represents the shear crack shape experienced in specimen PL20.0 (Fig. 3) which represents a lower boundary for crack propagation within the compression zone for the introduced test series since all other beams are designed with higher shear reinforcement ratios (Table 1). The derivation of a more general approach based on mechanical parameters (e.g. $\rho_w$ as proposed for members with stirrups in [34]) would be desirable, but the resulting kinematics at $V_{max}$ are highly influenced by the exact position at which the bent-up portion is crossed by the crack (e.g. crossing in the steep or flat part or crossing a second bent-up bar; see Section 4).

### 3.3. The relationship between the load and the width of the shear crack

The shear crack kinematics (*w*, *s*) at each point along a shear crack (A–B–F) can be defined by the rotation ψ of this crack around a centre of rotation which is defined to be crack tip F. This results in a horizontal opening of the crack to a width $u_A = \psi \cdot d_F$ at the height of the longitudinal reinforcement. Assuming that the width of the governing shear crack is proportional to the strains in the longitudinal reinforcement [38,34], a relationship between the crack width $u_A$ and the acting bending moment $M_F$ in each section can be written as [34]:

$$u_A = \frac{M_F}{A_s \cdot E_s} \cdot \frac{l_B}{d - c/3} \tag{2}$$

where *c* is the compression zones depth; *d* is the static depth; $l_B$ is the tributary length of all crack contributing to the governing shear crack; $A_s$ and $E_s$ is the cross-section and Young's modulus of the longitudinal reinforcement, respectively.

Eq. (2) has been derived for members with ribbed bars, assuming a tributary length of $l_B = d–c$ [34]. Based on the results of the presented test series, a modified tributary length of $l_{B,plain} = 1.6 \cdot (d–c)$ for members with plain bent-up bars is proposed. In simply supported beams subjected to point loads, $M_F$ can be expressed as $M_F = V \cdot a_F$, where $a_F$ is the horizontal distance between point F and the support (see Fig. 5a). As a result, the crack width $u_A$ is directly related to the acting shear force *V*, allowing a relationship between the load and the critical shear crack opening $V(u_A)$ to be formulated. The shear resistance can then be evaluated by equating this function with the shear resistance function.

### 3.4. Shear transfer mechanisms

With the kinematics defined at a certain crack location $x_A$, various constitutive models for shear transfer mechanisms that consider crack kinematics as input parameters can be utilised. The sum of these individual contributions ($V_i$) yields the shear resistance of the beam at the moment that the governing crack has opened to a given crack width ($u_A$). The shear resistance function can thus be written as $V_{Mod} = \Sigma V_i(u_A)$. Furthermore, the contribution of the compression chord has to be added, which was be estimated with an empirically derived formula [33]. It should be noted that the proposed approach is valid only for regions in which no direct struts are acting (e.g. not at region nearby point loads and bearings). Further, localised cracking does not occur if the shear crack opening is controlled by a high amount of ribbed shear reinforcement ($\rho_w > 0.3$ %). Therefore, the approach is valid only for low amount of shear reinforcement or if localised cracking is fostered due to the low bond characteristics of the plain bent-up bars (Fig. 3d). For the evaluation conducted in this study, the same constitutive laws [33,39,40,41,42] as those proposed in [34] were taken to calculate the contributions of the shear transfer actions attributed to the concrete (see Fig. 4a–c,f; equations given in Table 4). The contribution of the concrete compression strut ($V_{Compr}$) is determined by a semi-empirical approach

**Table 4**
Calculations of the contributions of the different shear transfer mechanisms.

| Shear-transfer action | Literature | Parameters |
|---|---|---|
| Residual tensile strength contribution $V_{Res}$<br>$V_{Res} = f_{ct}\cdot b\cdot\cos\beta_{BF}\cdot l_{F1}\cdot\left(1-\frac{1}{1+c_1}\cdot\left(\frac{u_A\cdot l_{F1}}{d_F\cdot w_c}\right)^{c_1}\right)$<br>with $w_c = G_F/f_{ct}\cdot(1+c_1)/c_1$ and $G_F = 0.073\cdot f_c^{0.18}$ | Tensile softening behavior [39];<br>Fracture energy $G_F$ [15] | $c_1$… constant (=0.31)<br>$l_{F1}$… length where $w < w_c$<br>$w_c$… maximum crack width for stress transfer<br>$f_c$… compressive strength of concrete<br>$f_{ct}$… tensile strength of concrete |
| Aggregate interlock $V_{Agg}$<br>$\frac{V_{Agg}}{\sqrt{f_c}\cdot b} = \sin\beta_{AB}\cdot\frac{c_3\cdot\bar{s}_A^{4/3}}{(c_2\cdot\bar{s}_A+0.8)\cdot\left(\frac{u_A}{d_F}\frac{c_2}{d_{dg}}\right)^{1.8+c_2\bar{s}_A}}\cdot\frac{l_2^{0.8+c_2\bar{s}_A}-l_1^{0.8+c_2\bar{s}_A}}{(l_2\cdot l_1)^{0.8+c_2\bar{s}_A}}$<br>$-\cos\beta_{AB}\cdot\frac{c_4\cdot\bar{s}_A^{7/3}}{(c_2\cdot\bar{s}_A+2)\cdot\left(\frac{u_A}{d_F}\frac{c_2}{d_{dg}}\right)^{3+c_2\bar{s}_A}}\cdot\frac{l_2^{2+c_2\bar{s}_A}-l_1^{2+c_2\bar{s}_A}}{(l_2\cdot l_1)^{2+c_2\bar{s}_A}}$<br>$+\cos\beta_{AB}\left[l_3\cdot\left(1-\frac{1}{1+c_1}\cdot\left(\frac{u_A\cdot l_3}{d_F\cdot w_c}\right)^{c_1}\right)-l_1\cdot\left(1-\frac{1}{1+c_1}\cdot\left(\frac{u_A\cdot l_1}{d_F\cdot w_c}\right)^{c_1}\right)\right]\cdot\frac{f_{ct}}{\sqrt{f_c}}$ | Two-phase aggregate interlock model [40] with modified kinematics according to [41] | $c_2$, $c_3$, $c_4$… constants<br>$\bar{s}_A = s_A/d_{dg}$<br>$s_A$… crack sliding at point A<br>$d_{dg}$… parameter to account for roughness<br>$f_c$… compressive strength of concrete<br>$f_{ct}$… tensile strength of concrete |
| Dowel action of the longitudinal reinforcement $V_{Dow}$<br>$V_{Dow} = k_b\cdot f_{ct}\cdot n\cdot(b/n-d_s)\cdot 2\cdot d_s$ | Approach of [42] | $k_b$… strength reduction factor for strained bars<br>$n$… number of bars<br>$d_s$… bar diameter<br>$f_{ct}$… tensile strength of concrete |
| Contribution of the compression zone $V_{Compr}$<br>$\frac{V_{Compr}}{V_c} = \frac{k_c\cdot h_f}{r_F} < 1$ | Approach of [33,34] | $k_c$… constant (=0.5) |
| Tension action of bent-up bars $V_{ST}$<br>$V_{ST} = \sum V_{ST,i} = \sum d_s\cdot\pi/4\cdot\sigma_{s,i}\cdot\sin\alpha_i$<br>and Eq. (3) for $\sigma_{s,i}$ | Tension chord model [43] for $\sigma_{s,i}$ and $\tau_{b,i}$ according to [43]; if not available from material tests | $d_s$… bar diameter<br>$\alpha_i$…bent-up bars angle<br>$\tau_{b,1}$… mean bond stress prior to yielding<br>$\tau_{b,1}$… mean bond after yielding<br>$E_s$ … Young's modulus of reinforcement<br>$f_y$… yield strength of reinforcement |
| Dowel action of bent-up bars $V_{SD}$<br>$V_{SD} = \sum V_{SD,i} = \sum V_{F,i}\cdot\cos\alpha_i$<br>and Eq. (4) for $V_{F,i}$ | Dowel action $V_{F,i}$ according to [15] based on [44] | $d_s$… bar diameter<br>$\alpha_i$…bent-up bars angle<br>$f_c$… compressive strength of concrete<br>$f_y$… yield strength of reinforcement<br>$s_{max}$… the slip at $V_{F,max}$ (between $0.1\cdot d_b$ and $0.2\cdot d_b$)<br>$\kappa_{2,max} \leq 1.6$ is the interaction coefficient for flexural resistance at $s_{max}$ |

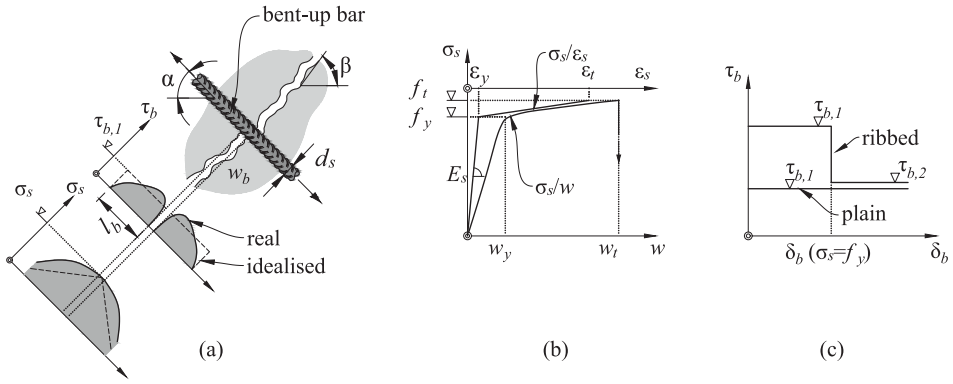


**Fig. 6.** Contribution of the bent-up bar under tension [43]: (a) stress state and bond behaviour of an embedded reinforcing bar; (b) stress vs crack opening behaviour of a reinforcing bar; (c) assumed rigid–plastic bond behaviour.

of Cavagnis [33,34], the residual tensile stresses at crack tip ($V_{Res}$) are calculated based on the tension softening-law of Reinhardt et al [39] (with the fracture energy acc. to fib Model Code [15]), the equations for aggregate interlock ($V_{Agg}$) are based on the two-phase model of Walraven [40] with modified kinematics for contact zone evaluation [41] and the dowel action of the longitudinal bars ($V_{Dow}$) by the approach of Fernández-Ruiz et al. [42]a

The contributions of the aforementioned mechanisms are supplemented by the contribution of the bent-up bars by tension action and dowel action (see Fig. 4e,f and Fig. 6). The contribution of tension action is calculated using the tension-chord model developed by Marti et al. [43], employing a simplified, stepped and rigid bond law [43] (Fig. 6c) and a bilinear stress–strain relationship for steel (Fig. 6a). For any given crack width, it is possible to obtain the stress state $\sigma_s$ in the reinforcing bar:

$$w_b = 2\cdot\delta\cdot\left(1+\frac{\sigma_s}{E_s}\right) \text{ and } \delta = \frac{d_s}{4}\int_0^{\sigma_s}\frac{1}{\tau_{b,i}(\sigma_s)}\cdot\varepsilon_s(\sigma_s)d\sigma_s \quad (3)$$

where $d_s$ and $E_s$ are the diameter and the Young's modulus of the bent-up bar, respectively. The bond-slip $\delta$ can be determined by integrating steel strains $\varepsilon_s$ along the bar. For an ordinary reinforcing bar, the

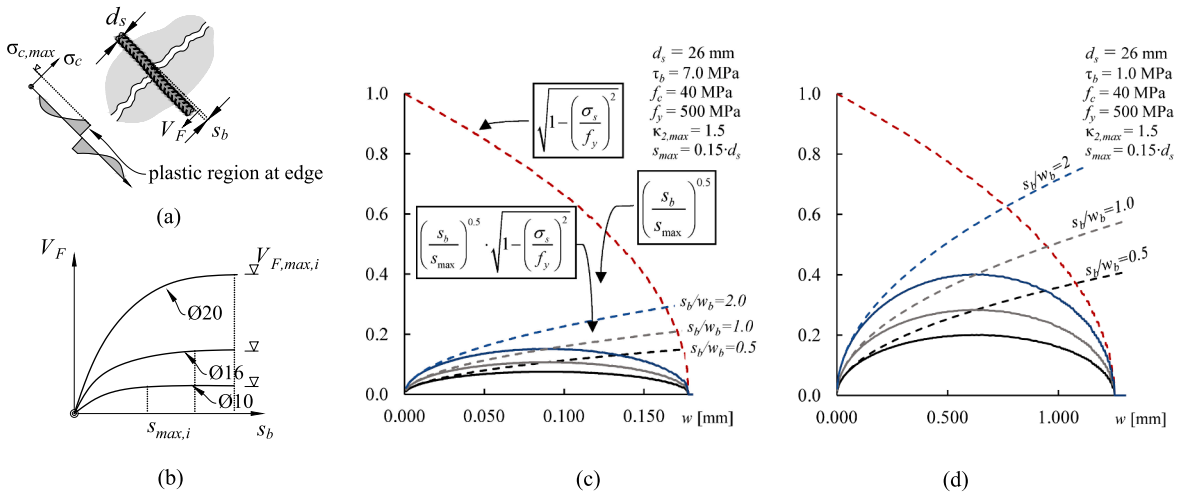


**Fig. 7.** Contribution of the bent-up bar as shear dowel [44]: (a) stress state of the surrounding concrete; (b) dowel force vs slip behaviour of an embedded bar; dowel activation in interaction with normal stress for (c) ribbed and (d) plain reinforcing bars.

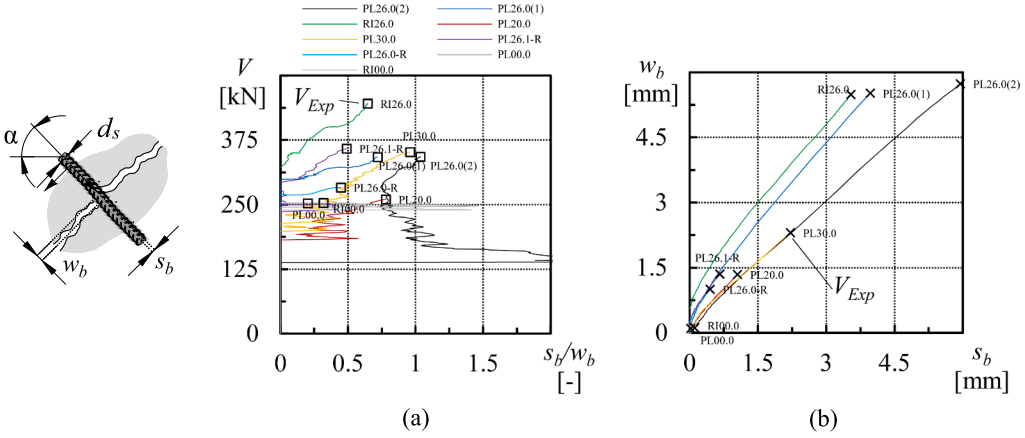


**Fig. 8.** Kinematics $s_b$ and $w_b$ for specimens that failed in shear: (a) development of the ratio $s_b/w_b$ during testing; (b) relationship between $w_b$ and $s_b$.

mean bond stress is calculated with $\bar{\tau}_b = \tau_{b,1} = 0.6 \cdot f_c^{2/3}$ prior to yielding and after onset of yielding with$\tau_{b,2} = 0.3 \cdot f_c^{2/3}$. The crack width in the direction of the bent-up bar can be calculated with $w_b = u_b \cdot \sin\alpha + v_b \cdot \cos\alpha = \psi(d_b \cdot \sin\alpha + l_b \cdot \cos\alpha)$ where $u_b = \psi \cdot d_b$, $v_b = \psi \cdot l_b$ and α is the bent-up bars angle (for $d_b$ and $l_b$ see Fig. 5b).

Along with the opening of this crack, a certain sliding perpendicular to the bar axis $s_b = \psi \cdot (d_b \cdot \cos\alpha - l_b \cdot \sin\alpha)$ occurs and causes dowel forces to be activated. To evaluate the contribution of dowel action, the shear dowel model of the fib Model Code 2010 [15] which was proposed by Randl [44] is taken (Fig. 7a + b). The same approach was used in [18,45] to evaluate the contribution of inclined shear reinforcement.

$$V_F(s_b) = V_{F,\max} \cdot \left(\frac{s_b}{s_{\max}}\right)^{0.5} \cdot \sqrt{1 - \left(\frac{\sigma_s}{f_y}\right)^2} \le \frac{A_s \cdot f_y}{\sqrt{3}} \text{ and } V_{F,\max} = \kappa_{2,\max} \cdot A_s \cdot (f_c \cdot f_y)^{0.5}, \quad (4)$$

where $s_{\max}$ is the sliding at $V_{F,\max}$ (between $0.1 \cdot d_s$ and $0.2 \cdot d_s$) and $\kappa_{2,\max} \le 1.6$ is the interaction coefficient for flexural resistance at $s_{\max}$. The interaction coefficient depends on the roughness conditions in the crack planes and lies within the range of 1.5 (very smooth) to 0.9 (very rough).

The dowel force $V_F$ is directly related to the offset of the bar axis: $(s_b/s_{\max})^{0.5}$ in Eq. (4) (Fig. 7b). The factor $(1\text{-}(\sigma_s/f_y)^2)^{0.5}$ in Eq. (4) accounts for reduced dowel force in bars under tension. The possible activation of the dowel ($V_F$ / $V_{F,\max}$) in beams with ribbed or plain bars is analysed in Fig. 7c and 7d, respectively. The normal stress is estimated with Eq. (3). Accounting for the proposed crack shape, the crack sliding $s$ is in the range of the crack width ($s \approx w$) in the portion A–B (Fig. 5b + c) which results in $s_b/w_b$ = 0.5–1.0 with respect to the direction of a 45° inclined bent-up bar. The given range is supported by DIC measurements at specimens which failed in shear (Fig. 8a + b). The kinematics ($s_b$, $w_b$) in Fig. 8 were determined at the crossing of the crack with the bent-up bar, while the kinematics of the governing shear cracks of specimens without shear reinforcement (PL00.0 and RI00.0) were determined at $d/2$ and were added for comparison reasons.

The results show that the contribution of the shear dowel is rather limited, since relatively strong sliding is necessary for full activation and the resulting normal stress $\sigma_s$ significantly lowers the contribution of the dowel. Assuming crack opening characteristics in the range $s_b/w_b = 1$, a maximum of 10 % and 25 % activation of the shear dowel could occur for a ribbed and plain reinforcing bar with the same yielding point, respectively. These values can only be achieved as soon as half of the yielding stress has been reached. For example, the use of a Ø26 mm bar ($\sigma_s = 0.5 \bullet f_y = 250$ MPa) results in a tension force of 133 kN but a maximum dowel force of only $0.25 \bullet V_{Fmax} = 24$ kN (133/24 = 5.5). In order to estimate their contributions to the shear strength of beams, both actions are multiplied by trigonometric functions: $V_{ST} = d_s \cdot \pi/4 \cdot \sigma_{s,i} \cdot \sin\alpha_i$ and $V_{SD} = V_F \cdot \cos\alpha_i$. As can be seen, the tension force is always more relevant for the shear capacity since both actions (tension and dowel

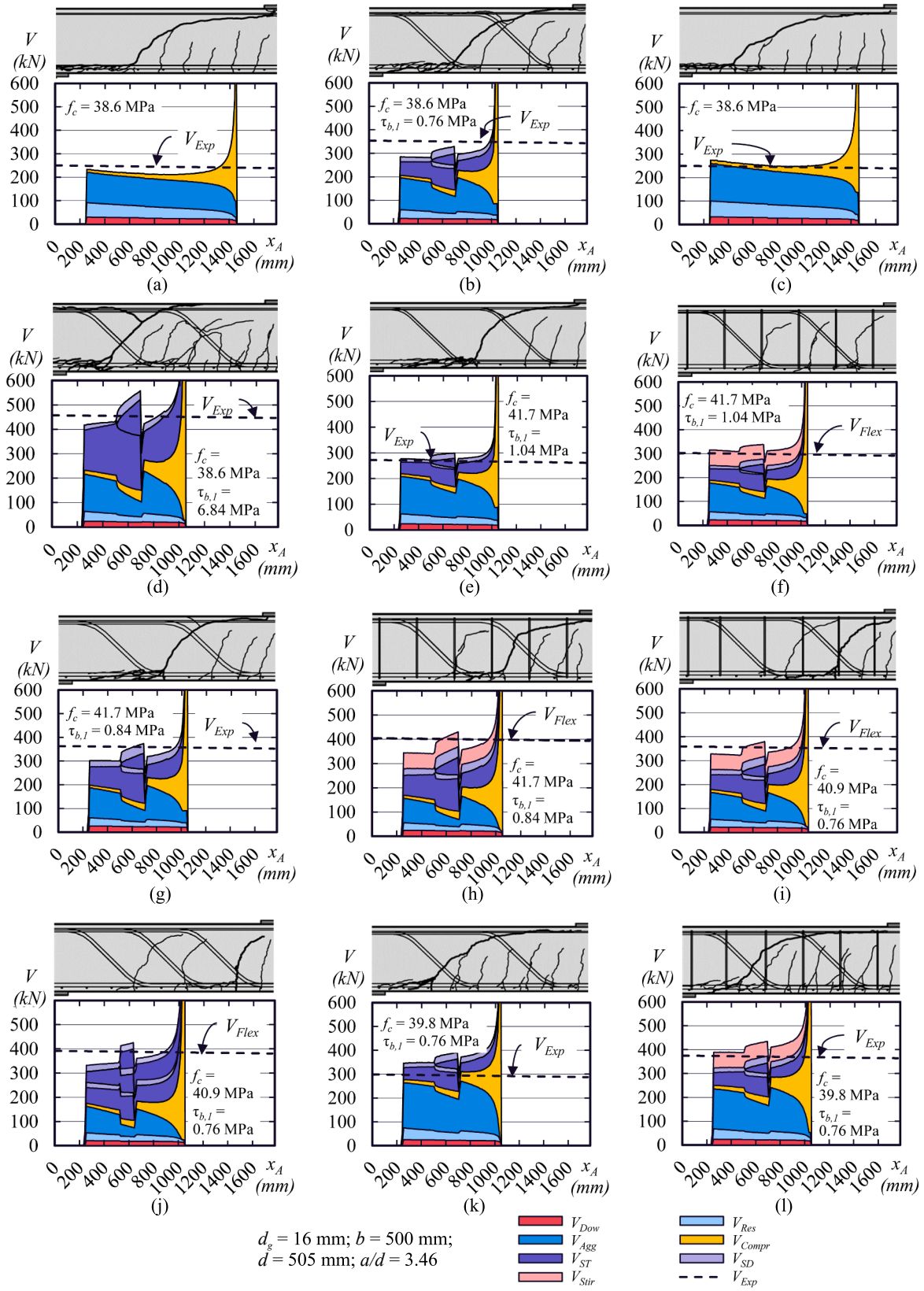


**Fig. 9.** Recalculation of specimens by the proposed model approach: (a) PL00.0; (b) PL26.0; (c) RI00.0; (d) RI26.0; (e) PL20.0; (f) PL20.1; (g) PL30.0; (h) PL30.1; (i) PL26.1; (i) PL26.0–n; (j) PL26.0–R; (l) PL26.1–R.

**Table 5**
Comparison of the experimental results (shear strength, crack width and activation of the bent-up bar) and the model predictions.

| | | Model predictions | | | Experimental results | | | Comparison | | |
|---|---|---|---|---|---|---|---|---|---|---|
| Specimen | $x_A$ (mm) | $u_A$ (mm) | $V_{ST}$ (kN) | $V_{Mod}$ (kN) | $u_{A,DIC}$ (mm) | $V_{ST,SG}$ (kN) | $V_{Exp}$ (kN) | $u_{A,DIC}/u_A$ | $V_{ST,SG}/V_{ST}$ | $V_{Exp}/V_{Mod}$ |
| PL00.0 | 606 | 0.356 | — | 219.1 | 0.34 | — | 252.6 | 0.96 | — | 1.15 |
| PL26.0 | 700 | 1.352 | 89.4<br>46.9 | 333.2 | 1.92 | 106.9<br>[a] | 342.5 | 1.42 | 1.20 | 1.03 |
| RI00.0 | 655 | 0.271 | — | 253.3 | 0.335 | — | 253.4 | 1.24 | — | 1.00 |
| RI26.0 | 440 | 0.908 | 197.8 | 426.9 | 0.91 | 215.2 | 445.5 | 1.00 | 1.09 | 1.04 |
| PL20.0 | 830 | 1.09 | 46 | 284 | 1.19 | 49.5 | 260.7 | 1.09 | 1.08 | 0.92 |
| PL30.0 | 855 | 1.071 | 68 | 331.6 | 1.71 | 87.4 | 351.9 | 1.60 | 1.29 | 1.06 |
| PL26.0–R | 470 | 0.753 | 60.8 | 346.1 | 0.66 | [a] | 283.6 | 0.88 | — | 0.82 |
| PL26.1–R | 440 | 0.826 | 62.7 | 388.4 | 0.91 | [a] | 360 | 1.10 | — | 0.93 |
| | | | | | | | m | 1.16 | 1.161 | 0.994 |
| | | | | | | | COV | 0.211 | 0.085 | 0.104 |

[a] No measurements available.

action) contribute equally to the shear strength of beams with bent-up bars inclined at α = 45° (Fig. 4d–e).

### 3.5. Solution procedure and application to beams with bent-up bars

The shear capacity needs to be obtained iteratively for every possible location of crack origin $x_A$ with the lowest shear capacity exhibited defining the shear strength of the member. The iterative procedure for calculation of the shear capacity [34] contains the following steps:

(1) Choose a location of the shear crack $x_A$.

(2) Calculate the angle $\beta_{AB}$ as a function of $\alpha_A = M_A/(V_A \cdot d)$ according to Eq. (1) (refer to Fig. 5).

(3) Assume an initial crack opening $u_{Ai}$.

(4) Calculate, as a function of the shape of the crack and its kinematics, the residual tensile strength force ($V_{Res}$), the aggregate interlock force ($V_{Agg}$), the dowel action ($V_{Dow}$), the contribution of the compression zone ($V_{Compr}$) and the tensile force ($V_{ST}$) and dowel action ($V_{SD}$) of the bent-up bar with the equations given in Table 4 and the shear capacity as the sum of these contributions ($V_{Mod} = \Sigma V_i(u_A)$)

(5) Calculate the crack opening $u_A$ as a function of the acting bending moment at the section corresponding to the tip of the crack ($M_F$) according to Eq. (2), where $M_F$ is proportional to the shear force ($V$).

(6) Iterate the crack opening $u_{Ai}$ at step 3 and repeat from step 3 to 6, until $u_A$ is equal to $u_{Ai}$ which gives a critical shear crack width. The

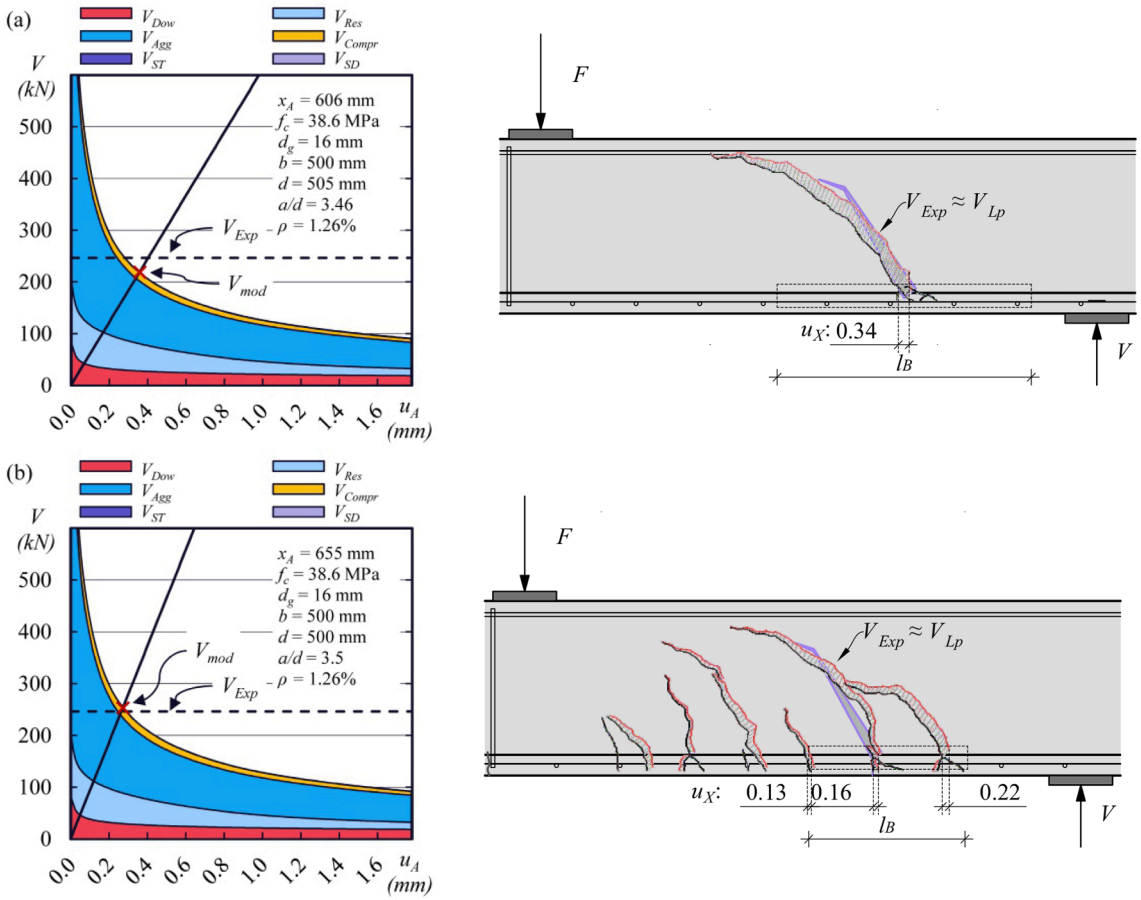


**Fig. 10.** Contribution of the shear transfer mechanisms, intersection of the load–deformation relationship with the failure criterion and comparison with the experimental results, and crack kinematics and horizontal opening $u$ of the cracks contributing to the opening of the governing shear crack in a region of length $l_B$ for specimen (a) PL00.0 and (b) RI00.0.

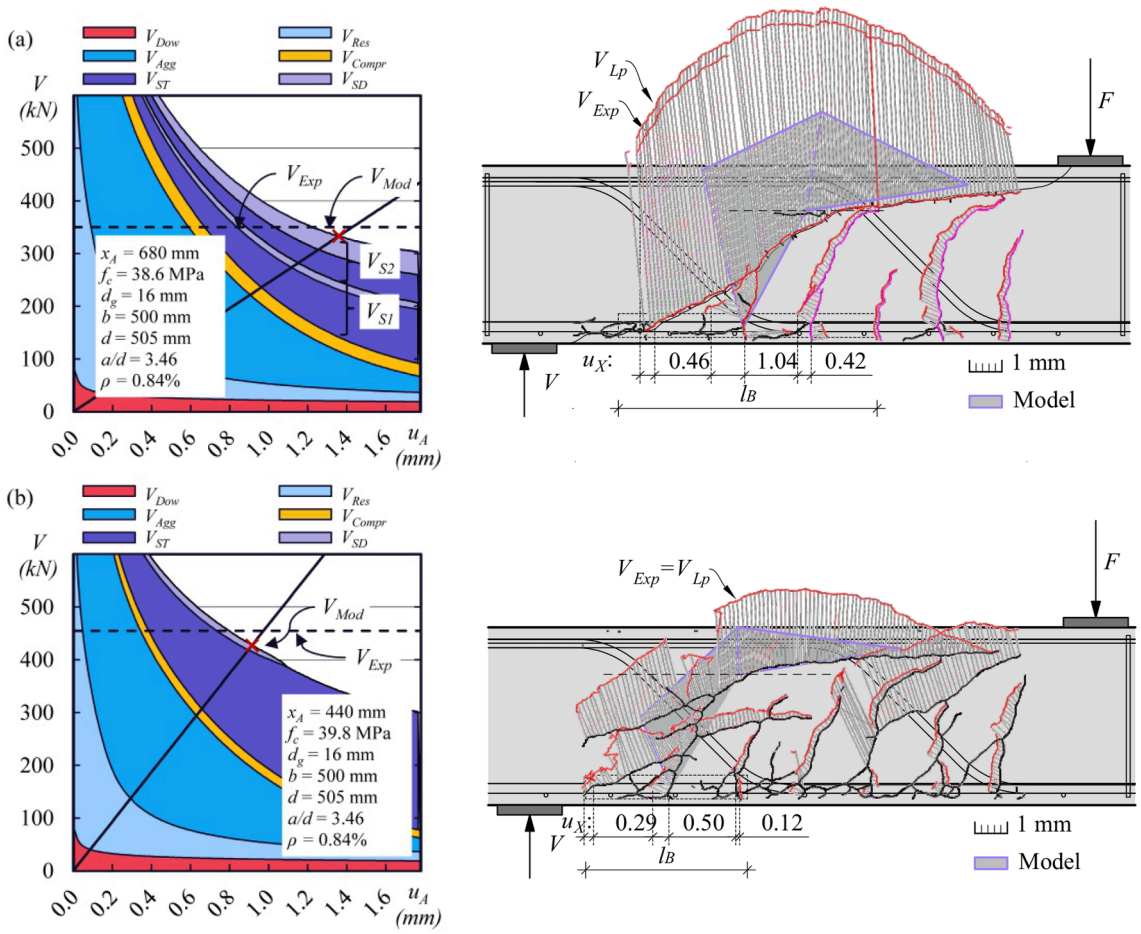


**Fig. 11.** Contribution of the shear transfer mechanisms, intersection of the load–deformation relationship with the failure criterion and comparison with the experimental results, and crack kinematics and horizontal opening $u$ of the cracks contributing to the opening of the governing shear crack in a region of length $l_B$ for specimen (a) PL26.0 and (b) RI26.0.

reaching of this width marks the state were unstable crack propagation leads to the subsequent collapse of the member and is in accordance to the assumptions of the critical shear crack theory [38]. The evaluation of the proposed approach is shown for all specimens in Fig. 9.

The model shows that the higher activation of the shear reinforcement (tension and dowel action of bent-up bars or stirrups) decreases the relative contributions of the shear transfer actions attributed to the concrete (aggregate interlock and residual tensile stresses in the fracture process zone). It was shown in [33] that for members without shear reinforcement, the governing location of $x_A$ could be adequately described with a fixed location of $x_A = a/2$ since the calculated shear strength is approximately the same around this point (see also Fig. 9a + c). However, for members with bent-up bars, the calculated shear strength is strongly influenced by the reinforcement layout, which is why every location $x_A$ should be checked (Fig. 9b,d–l). For the investigated reinforcement layout, a region of higher shear capacity is calculated around $x_A$ = 600 mm due to the crossing of several bent-up bars and a region with a lower shear strength closer to the support. Therefore, the crack position may become relevant as can be illustrated by the comparison of tests with different bar surface types for the longitudinal reinforcement. Specimen PL26.0–R with ribbed longitudinal reinforcement and plain bent-up bars exhibited a lower shear capacity as their counterpart with plain longitudinal reinforcement (PL26.0). While no flexural cracking in regions close to the support was observed in beams with plain longitudinal reinforcement (Fig. 9a,b,e–j), the governing cracks originated closer to the supports in beams with ribbed longitudinal reinforcement (Fig. 9c,d,k,l).

## 4. Discussion by comparison model to test results

In this section, the proposed modelling approach is evaluated for all tested specimens that exhibited shear failure. The origin of the evaluated crack ($x_A$) was chosen according to the observed crack pattern (Fig. 3d). The model predictions for the identified crack kinematics ($u_{A,DIC}$), strain gauge measurements ($V_{ST,SG} = \varepsilon_{s,SG} \bullet E_s \bullet A_s \bullet \sin\alpha$) and shear strength $V_{Exp}$ are also compared. It should be noted that the geometry of the bent-up bars is modelled without the curved top and bottom ends of the inclined part. As a result, (3) and (4) would provide incorrect contributions if the bent-up bars crossed at the very tip of the crack due to the incorrect inclination $\alpha_i$. Furthermore, the resulting contributions in this region are rather low due to the small kinematics. For the sake of simplicity, the contributions of the bent-up bars are only considered if crossed within $l_F = d–c$ (Fig. 5a). The results are listed in Table 5.

The approach yields accurate results in predicting the shear strength ($V_{Exp}/V_{Mod}$: $m$ = 0.994; COV = 0.104) and the contribution of the bent-up bar ($V_{ST,SG}/V_{ST}$: m = 1.161; COV = 0.085) at the same time. Overall, there is more scatter in the comparison of the model approach with the crack kinematics ($u_{A,DIC}/u_A$: $m$ = 1.160; COV = 0.211). With respect to the crack shape (Figs. 10–13), the quasi-horizontal portion (B–F) appears to be longer when larger amounts of shear reinforcement are crossed (PL26.0, RI26.0, PL30.0, PL26.1–R). The experimental and analytical crack shape and resulting kinematics agree well in the specimens without shear reinforcement (XX0.00), PL20.0 and PL26.0–R.

As for the effect of the type of longitudinal reinforcement (RI00.0 or PL00.0), no differences in the test results were observed ($V_{Exp}$, $u_{A,DIC}$).

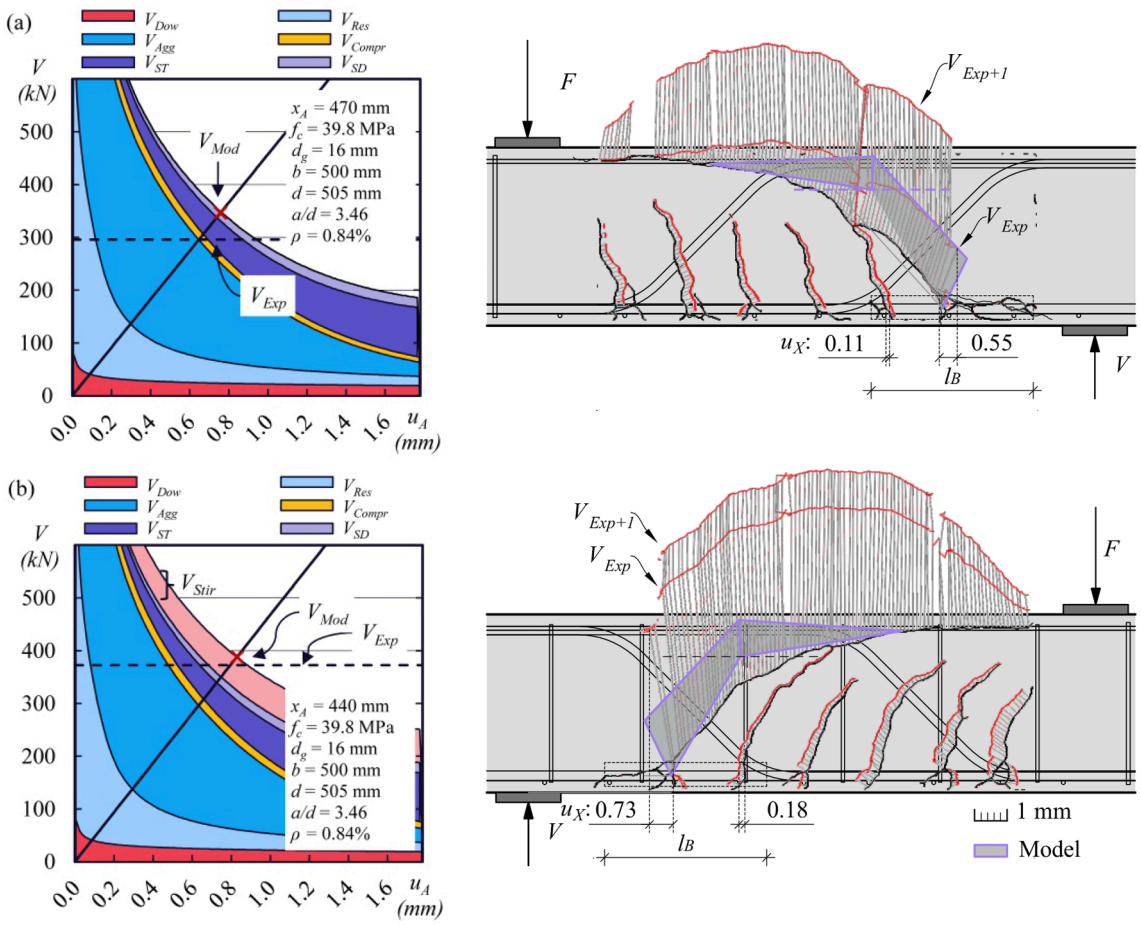


**Fig. 12.** Contribution of the shear transfer mechanisms, intersection of the load–deformation relationship with the failure criterion and comparison with the experimental results, and crack kinematics and horizontal opening $u$ of the cracks contributing to the opening of the governing shear crack in a region of length $l_B$ for specimen (a) PL26.0–R and (b) PL26.1–R.

Nevertheless, a different tributary length $l_B$ was used for the two specimens to account for the different bond behaviour, resulting in a different inclination in the load–shear crack width curve (Fig. 10a and b). In specimen RI00.0, the prediction of $V_{Exp}$, matches the test result while the crack width $u_{A,DIC}$ is overestimated. Just the opposite is true for specimen PL00.0, where the crack width $u_{A,DIC}$ matches the observations while the shear strength is underestimated.

As for the effect of the type of bent-up reinforcement (RI26.0 and PL26.0), the model approach correctly estimates the shear capacity $V_{Exp}$ in both cases, even though different tributary lengths and bond behaviours of the bent-up bar types were assumed. It should be noted that in specimen PL26.0, two bent-up bars crossed the governing shear crack. Due to its weaker bond properties, the bar in beam PL26.0 did not yield in the experiment ($V_{ST,SG}$ / $V_{ST,y,Ø26\text{-}S235}$ = 106.9 / 114.1 = 0.94), even though the crack kinematics were more pronounced ($u_{A,DIC}$ and Fig. 11). This was also predicted by the model ($V_{ST}$ = 89.4 kN). In specimen RI26.0, on the other hand, yielding of the bent-up bar was confirmed by measurements, while the predicted contribution to the shear strength was lower than the measured value ($V_{ST}$ / $V_{ST,y,Ø26\text{-}B550B}$ = 197.8 / 215.5 = 0.92). The crack kinematics are underestimated in both cases: longer sections B–F are predicted, resulting in different centres of rotation. It should be noted, that the contribution of dowel action of the bent-up bar may be lower than calculated, if pronounced transverse cracking along the bent-up bar occurs (e.g. Pl26.0 and RI26.0 in Fig. 11).

Specimen PL26.0–R with hybrid longitudinal reinforcement was analysed with a tributary length proposed for ribbed bars ($l_B$ = $d$–$c$), since only ribbed reinforcement was located at the observed crack origin. The model correctly predicts $u_A$ at $V_{Exp}$ to be smaller than in PL26.0 and RI.26.0. The shear capacity is overestimated by the model ($V_{Exp}/V_{Mod}$ = 0.82), which can be due to the flatter crack shape, as this is likely to result in a smaller contribution of aggregate interlock to the shear strength. To account for the observed crack shape, a second analysis assuming $l_F$ = 0.6•$d$ and $\beta_{AB}$ = 48° was conducted but only yields a slightly better prediction, since the contribution of a second bent-up bar is considered ($V_{Exp}/V_{Mod}$ = 283.6 / 331.6 = 0.86). The presence of additional stirrups is analysed for specimen PL26.1–R, which is the only specimen with stirrups that failed in shear. The stirrups were modelled assuming that they yielded and contributed to the shear strength within the horizontal length of the idealised crack A–B–F. As a result, the total contribution of the stirrups to the shear strength $V_{Stir}$ = 63.0 kN agrees with the difference between the beams observed in the tests (+76.4 kN compared to PL26.0–R). While the shear capacity was predicted quite accurately, the assumed kinematics were too small (Fig. 12).

As far as the amount of shear reinforcement is concerned (Pl20.0, PL26.0 and PL30.0), the model approach accurately predicts the shear capacity $V_{Exp}$. Furthermore, the model provides an explanation for the slightly smaller shear capacity of PL26.0 compared to PL30.0, since in PL26.0 two bars cross the governing crack (Fig. 11a), while in PL30.0 only one bar crosses the crack (Fig. 13b). The observed crack kinematics as well as the contribution of the bent-up bar of specimen PL20.0 are reproduced perfectly by the model, while those of PL30.0 are underestimated (Table 5). It is important to note that the bent-up bars of specimens PL20.0 and PL30.0 were not utilised until the yield point

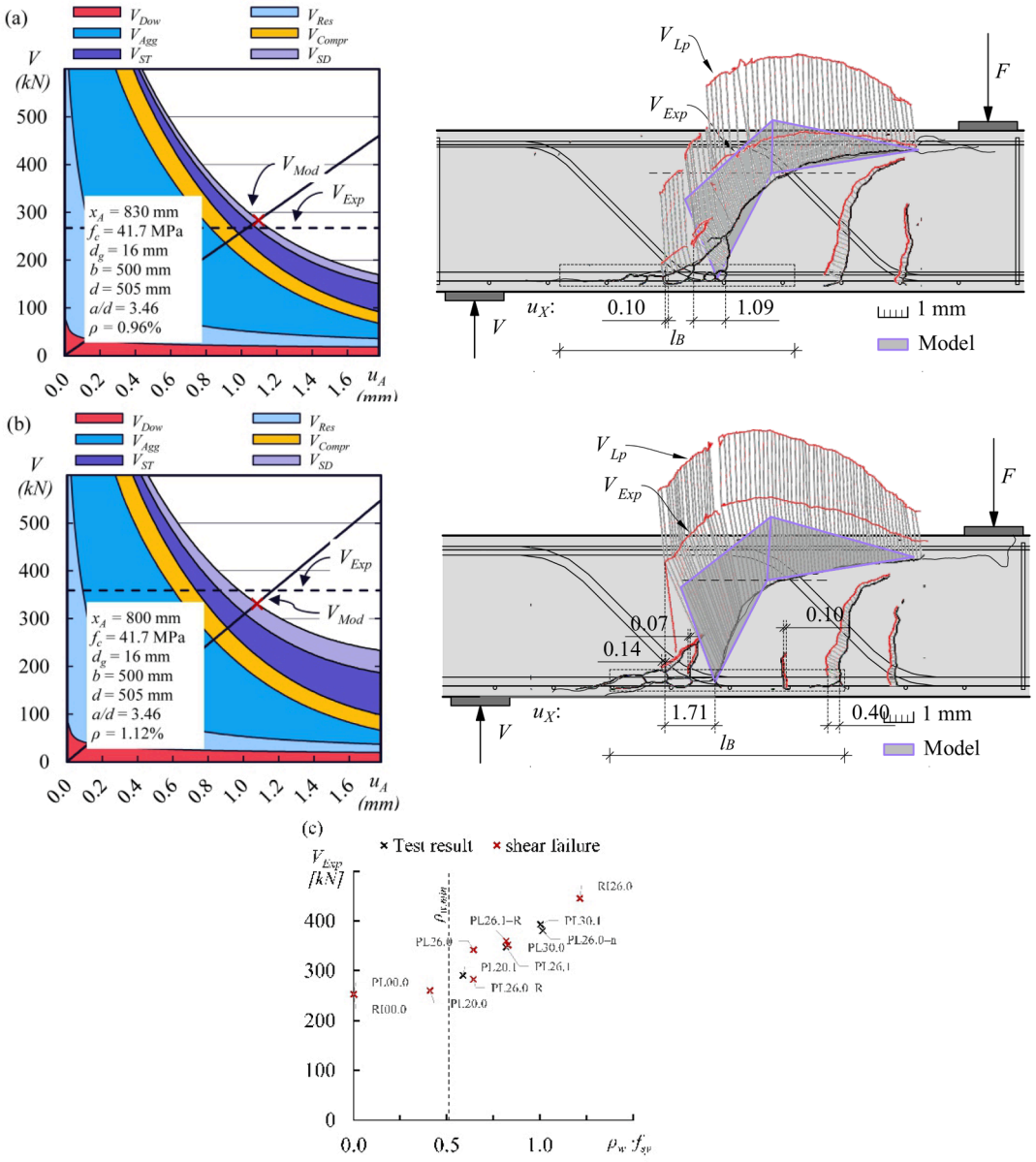


**Fig. 13.** Contribution of the shear transfer mechanisms, intersection of the load–deformation relationship with the failure criterion and comparison with the experimental results, and crack kinematics and horizontal opening $u$ of the cracks contributing to the opening of the governing shear crack in a region of length $l_B$ for specimen (a) PL20.0; (b) PL30.0; (c) influence of the shear reinforcement ratio on the shear capacity.

(utilisation rate based on strain gauge measurements: $V_{ST,SG}$ / $V_{ST,y,Ø20\text{-}S235}$ = 49.5 / 72.9 = 0.68; $V_{ST,SG}$ / $V_{ST,y,Ø30\text{-}S235}$ = 87.4 / 146.9 = 0.60), which was also calculated by the model (see Table 5). Overall, the shear reinforcement ratio shows an almost linear positive correlation with the shear capacity (Fig. 13c).

## 5. Summary and conclusions

This paper presents the experimental investigations and mechanical modelling of the shear strength of members with ribbed and plain bent-up bars that exhibit localised cracking. By extending a model for failures in shear of members without shear reinforcement with constitutive laws from the literature to estimate the contributions to the shear strength of bent-up bars, it was possible to validate relevant test results. Based on the findings of this analysis the following conclusions are drawn:

- Plain bent-up bars contribute to the shear capacity despite their weaker bond properties, as shown by the higher shear capacities of beams with this type of reinforcement compared to their reference beams without any shear reinforcement. An almost linear increase in capacity with increasing shear reinforcement ratio was observed.
- The bond qualities of the longitudinal reinforcement and the resulting effect on the cracking patterns can influence the shear capacity of beams with bent-up bars, as shown by a comparison of a beam with ribbed longitudinal reinforcement and plain bent-up bars to a beam with plain reinforcing bars only, which exhibited a higher shear capacity. The crack patterns showed pronounced shear cracking in beams with plain longitudinal reinforcing bars, with generally fewer flexural cracks in the testing area compared to beams with ribbed longitudinal reinforcement. Consequently, the origin of the governing cracks moved closer to the supports in beams with ribbed longitudinal reinforcement in which a lower shear capacity was attributed to a governing crack according to the proposed modelling approach. Similar effects on the origin of the governing crack caused by the surface type of the longitudinal reinforcement was observed for beams designed without bent-up bars. However,

the shear capacity of the tested members without shear reinforcement was not influenced in the present test series, as the shear capacity according to the modelling approach is approximately the same at both positions.

- The presented mechanical modelling approach based on the evaluation of various shear transfer mechanisms in an idealised shear crack adequately describes the structural behaviour of beams with localised shear cracking, predicting the shear capacity, the crack kinematics and the utilisation of the bent-up bars. The model shows that the activation of the shear reinforcement (tension and dowel action) decreases the relative contributions of the shear transfer actions attributed to the concrete (aggregate interlock and residual tensile stresses in the fracture process zone).
- The contribution of a bent-up bar to shear capacity can be described by kinematics in a shear crack. In the tested members with plain bent-up bars, the reinforcing bars were not utilised until the yield point. This was also confirmed by the results of the recalculation of the introduced modelling approach. An evaluation based on the kinematics shows that tension action generally contributes more to the shear capacity than dowel action.

## CRediT authorship contribution statement

**Tobias Huber:** Conceptualization, Methodology, Formal analysis, Funding acquisition, Project administration, Investigation, Visualization, Writing - original draft, Writing - review & editing. **Franz Untermarzoner:** Investigation, Writing - review & editing. **Johann Kollegger:** Writing – review & editing, Supervision.

## Declaration of Competing Interest

The authors declare that they have no known competing financial interests or personal relationships that could have appeared to influence the work reported in this paper.

## Data availability

Data will be made available on request.

## Acknowledgments

The authors would like to acknowledge the financial support of the infrastructure operators ÖBB-Infrastruktur AG (grant number: HLK/4300875857), DB Netz AG (grant number: 10849270) and Asfinag Baumanagement GmbH (grant number: 302204592) and the fruitful cooperation with all parties involved. The authors would further like to thank Alfred Trepka GmbH for the excellent and thoughtful production of the specimens. The authors acknowledge TU Wien Bibliothek for financial support through its Open Access Funding Programme

## References

[1] Mörsch E. Der Eisenbetonbau, seine Theorie und Anwendung. Stuttgart: K. Wittwer Verlag; 1908.
[2] Bach, C., Graf O.: „Versuche mit Eisenbeton-Balken zur Ermittlung der Widerstandsfähigkeit verschiedener Bewehrung gegen Schubkräfte - zweiter Teil“. In: Deutscher Ausschuss für Eisenbeton 12, (1911).
[3] Bach, C., Graf O.: „Versuche mit Eisenbeton-Balken zur Ermittlung der Widerstandsfähigkeit verschiedener Bewehrung gegen Schubkräfte - dritter Teil“. In: Deutscher Ausschuss für Eisenbeton 20, (1912).
[4] Richart FE. An investigation of web stresses in reinforced concrete beams. University of Illinois; 1927. Doctoral thesis.
[5] Leonhardt, F., Walther, R.: Schubversuche an Plattenbalken mit unterschiedlicher Schubbewehrung. Deutscher Ausschuss für Stahlbeton (in German), Vol. 156. Ernst & Sohn, Berlin, (1963), 1–84.
[6] Özden K. An Experimental Investigation on the Shear Strength of Reinforced Concrete Beams: Tests Performed at Structural Research Laboratory, Technical University of Denmark. Istanbul: Technical University of Istanbul Faculty of Civil Engineering; 1967. p. 1–243.
[7] Leksukhum, K. und R. Smith.: Comparative Study of Bent-up Bars with other Forms of Secondary Reinforcement in Beams. In: ACI Special Publication 68.1 (1971), 32–35.
[8] Regan P, Khan M. Bent-Up Bars as Shear Reinforcement. ACI 1974;42:249–66.
[9] Johansen K. Critical remarks on the effect of bent-up bars and stirrups in reinforced concrete beams. 5th IABSE Congress Lisbon 1956, Final Report, (1957), 507–512.
[10] Sørensen HC. Efficiency of bent-up bars as shear reinforcement. Special Publication 1974;42:267–84.
[11] Pedersen, C.: Shear in beams with bent-up bars. In IABSE Colloquium, Copenhagen, (1979), Session II, Plasticity in Reinforced Concrete 79–86.
[12] ACI (American Concrete Institute) ACI 318-19: Building code requirements for structural concrete and commentary, American Concrete Institute, Farmington Hills, MI, USA, (2019).
[13] CEN. 2005. EN1992-1-1 Eurocode 2 Design of concrete structures – Part 1-1: General Rules and Rules for Buildings. Brussels: Comité Européen de Normalisation.
[14] CSA Committee A23.3: “Design of Concrete Structures,” CSA Group, Toronto, ON, Canada, (2004), 240 ff.
[15] fib – Fédération Internationale du Béton: fib Model Code for Concrete Structures 2010. Ernst & Sohn, October (2013).
[16] Huber, T.: Assessment of the shear resistance of existing reinforced concrete bridges with bent-up bars. Doctoral thesis, TU Wien, (2019).
[17] Huber T, Huber P, Kollegger J. Shear strength model for existing RC components with bent-up bars (in German). Beton- Stahlbetonbau 2020;10(115):811–20.
[18] Huber T, Huber P, Fasching S, Vill M, Kollegger J. Shear behavior of RC components with bent-up bars based on photogrammetric measurements“. (in German) Bauingenieur 95 2020;6:181–93.
[19] CEB-FIP Model Code for Concrete Structures 1978. Comité Euro-International du Béton (CEB), Lausanne, (1978).
[20] ÖN B 4008-2: Assessment of load capacity of existing structures – Part 2: Bridge construction. Austrian Standards International, Vienna, (2019).
[21] TC RILEM.: RILEM recommendations for the testing and use of constructions materials. RC 6 bond test for reinforcement steel. 2. Pull-out test (1983), 218–220.
[22] Gehri N, Mata-Falcón J, Kaufmann W. Automated crack detection and measurement based on digital image correlation. Constr Build Mater 2020;256.
[23] Gehri N, Mata-Falcón J, Kaufmann W. Refined extraction of crack characteristics in large-scale concrete experiments based on digital image correlation. Eng Struct 2022;251.
[24] Fédération Internationale du Béton (fib): Towards a rational understanding of shear in beams and slabs (workshop proceedings), fib Bulletin, Vol. 85 (2018), 1–338.
[25] Hegger J, Görtz S, Schwermann R. Analysis of shear-cracking behaviour using photogrammetry (in German). Bautechnik 2002;79(3):135–43.
[26] Cavagnis F, Ruiz MF, Muttoni A. Shear failures in reinforced concrete members without transverse reinforcement: An analysis of the critical shear crack development on the basis of test results. Eng Struct 2015;103:157–73.
[27] Huber P, Huber T, Kollegger J. Investigation of the shear behavior of RC beams on the basis of measured crack kinematics. Eng Struct 2016;113:41–58.
[28] Campana S, Fernandez Ruiz M, Anastasi A, Muttoni A. Analysis of shear-transfer actions on one-way RC members based on measured cracking pattern and failure kinematics. Mag Concr Res 2013;65(5-6):386–404.
[29] Cavagnis F, Ruiz MF, Muttoni A. An analysis of the shear-transfer actions in reinforced concrete members without transverse reinforcement based on refined experimental measurements. Struct Concr 2018;19(1):49–64.
[30] Huber P, Huber T, Kollegger J. Influence of loading conditions on the shear strength of post-tensioned beams with low shear reinforcement ratios. Eng Struct 2018;170:91–102.
[31] Huber T, Huber P, Kollegger J. Influence of aggregate interlock on the shear resistance of reinforced concrete beams without stirrups. Eng Struct 2019;186:26–42.
[32] Huber, P., Kromoser, B., Huber, T., Kollegger, J.: Approach for the determination of the shear strength of existing post-tensioned bridge girders with a minimum amount of transverse reinforcement (in German). Bauingenieur 91 (2016), Vol. 6, 227–237.
[33] Cavagnis F, Ruiz MF, Muttoni A. A mechanical model for failures in shear of members without transverse reinforcement based on development of a critical shear crack. Eng Struct 2018;157:300–15.
[34] Cavagnis, F.: Shear in reinforced concrete without transverse reinforcement: from refined experimental measurements to mechanical models. Doctoral thesis, Ecole Polytechnique Fédérale de Lausanne, (2017).
[35] Yang, Y.: Shear behaviour of reinforced concrete members without shear reinforcement: a new look at an old problem. TU Delft, Delft University of Technology, dissertation, 2014.
[36] Classen M. Shear Crack Propagation Theory (SCPT)–The mechanical solution to the riddle of shear in RC members without shear reinforcement. Eng Struct 2020;210.
[37] Tung ND, Betschoga C, Tue NV. Analysis of the crack development and shear transfer mechanisms of reinforced concrete beams with low amounts of shear reinforcement. Eng Struct 2020;222.
[38] Muttoni A, Fernandez Ruiz M. Shear strength of members without transverse reinforcement as function of critical shear crack width. ACI Struct J 2008;105(2):163–72.
[39] Reinhardt HW. Fracture mechanics of an elastic softening material like concrete. Heron 1984;29(2).
[40] Walraven JC. Fundamental analysis of aggregate interlock. In: ASCE Journal of Structural Division 1981;107(11):2245–70.

[41] Guidotti R.: Poinçonnement des planchers-dalles avec colonnes superposées fortement sollicitées. PhD thesis. Thesis no. 4812 (in French). Lausanne, Switzerland: Ecole Polytechnique Fédérale de Lausanne; (2010).
[42] Fernández Ruiz M, Mirzaei Y, Muttoni A. Post-punching behavior of flat slabs. ACI Struct J 2013;110:801–12.
[43] Marti P, Alvarez M, Kaufmann W, Sigrist V. Tension chord model for structural concrete. Struct Eng Int 1998;8(4):287–98.
[44] Randl N. Load Bearing Behaviour of Cast-in Shear Dowels (in German). Beton-Stahlbetonbau 2007;102(S1):31–7.
[45] Randl N, Kunz J. Bending Shear Tests on R/C-Beams with Post-Installed Shear Reinforcement (in German). Beton- Stahlbetonbau 2009;104(11):728–36.